Data in Brief 43 (2022) 108424

Contents lists available at ScienceDirect

Data in Brief

journal homepage: www.elsevier.com/locate/dib

Data Article

Dataset of Phanerozoic continental climate and Köppen–Geiger climate classes

Alexandre Pohl[a,b,*], Thomas Wong Hearing[c], Alain Franc[d], Pierre Sepulchre[e], Christopher R. Scotese[f]

[a] *Biogéosciences UMR 6282, Université Bourgogne Franche-Comté, CNRS/UBFC, France*
[b] *Department of Earth and Planetary Sciences, University of California, Riverside, CA, USA*
[c] *Department of Geology, Ghent University, 9000, Belgium*
[d] *BIOGECO, INRAE, Université de Bordeaux, Cestas, and Pleiade, EPC INRIA-INRAE, Université de Bordeaux, Talence, France*
[e] *Laboratoire des Sciences du Climat et de l'Environnement, LSCE/IPSL, CEA-CNRS-UVSQ, Université Paris-Saclay, Gif-sur-Yvette, France*
[f] *Department of Earth & Planetary Sciences, Northwestern University, Evanston, IL, USA*

ARTICLE INFO

Article history:
Received 15 April 2022
Revised 17 June 2022
Accepted 21 June 2022
Available online 27 June 2022

Keywords:
Paleoclimate
General circulation model
Phanerozoic
Continental climate
Seasonal temperatures
Seasonal precipitation
Seasonal evaporation
Köppen–Geiger climate classes

ABSTRACT

This article describes a suite of global climate model output files that provide continental climatic conditions (monthly temperatures, precipitation, evaporation, precipitation minus evaporation balance, runoff) together with the calculated Köppen–Geiger climate classes and topography, for 28 evenly spaced time slices through the Phanerozoic (Cambrian to Quaternary, 540 Ma to 0 Ma). Climatic variables were simulated with the Fast Ocean Atmosphere Model (FOAM), using a recent set of open-access continental reconstructions with paleotopography and recent atmospheric CO_2 and solar luminosity estimates. FOAM is a general circulation model frequently used in paleoclimate studies, especially in the Palaeozoic. Köppen–Geiger climate classes were calculated based on simulated temperature and precipitation fields using Wong Hearing et al.'s [1] implementation of Peel et al.'s [2] updated classification. This dataset provides a unique window onto changing continental climate throughout the Phanerozoic that accounts for the simultaneous evolution of paleogeography (continental configuration and topography),

* Corresponding author(s)
E-mail address: alexandre.pohl@u-bourgogne.fr (A. Pohl).

https://doi.org/10.1016/j.dib.2022.108424

atmospheric composition and greenhouse gas forcing, and solar luminosity.

Specifications Table

Subject	Earth and Planetary Sciences (General)
Specific subject area	Continental climate and Köppen–Geiger climate classes during the Phanerozoic (last 540 million years)
Type of data	NetCDF raster files [longitude × latitude (× time)] and CSV files
How data were acquired	General circulation model simulations conducted on high-performance computers of a regional cluster
Data format	Raw
Parameters for data collection	Geographic Coordinate System WGS1984 with 2.8° × 1.4° longitude-latitude spatial resolution
Description of data collection	General circulation model simulations using recent continental reconstructions and atmospheric CO_2 estimates and time-varying solar luminosity values
Data source location	Global scale (Entire World)
Data accessibility	Repository name: ZENODO Data identification number: doi:10.5281/zenodo.6620748 Direct URL to data: https://zenodo.org/record/6620748

Value of the Data

- This dataset comprises seasonal continental climatic fields and calculated Köppen–Geiger climate classes simulated over 28 evenly spaced (20 Myr) time slices covering the last 540 million years (Phanerozoic Eon), using time-evolving continental configurations, atmospheric CO_2 concentrations and solar luminosity values.
- The 28 NetCDF files provide valuable raster data for studies investigating long-term changes in continental climate in the deep time.
- Published rasters are based on the geodynamic model of Scotese and Wright [3], which also includes the rotation files required to calculate (in (py)GPlates) the paleo-coordinates of sampling points based on present-day longitude-latitude values. It is, thus, straightforward to calculate the paleo-locations of any data points and locate them on our maps of Phanerozoic environmental parameters.
- Our dataset is useful to non-climate modelling experts interested in integrating this type of data into their multidisciplinary studies.
- These data can be used as input for other models, such as ecological niche models and species distribution models. Climatic information can also be extracted for key localities and regions in order to place collected geological / biological data in a broader paleoclimatic context.

1. Data Description

The dataset comprises 28 files, named following the pattern: "[age]Ma_Pohletal2022_DIB_PhaneroContinentalClimate[extension]". "[age]" is the age of the considered time slice expressed in million years before present (Ma), from 540 Ma (Cambrian) to 0 Ma (Quaternary) (both included). "[extension]" is either ".nc" or ".csv", since files are provided in two file formats. NetCDF (extension ".nc") is a self-describing file format that can be read using scripting

Table 1
List of variables included in all files.

Label	Variable description	Unit
topo	Topography derived from the continental reconstructions of Scotese and Wright [3]	m above sea level
tssub1	Top layer soil temperature simulated in the FOAM model	°C
precip	Total precipitation (i.e., convective and large-scale, liquid and solid) simulated in the FOAM model	mm day^{-1}
evp	Evaporation simulated in the FOAM model	mm day^{-1}
rnf	Runoff simulated in the FOAM model	mm day^{-1}
PmE	Precipitation minus evaporation balance simulated in the FOAM model	mm day^{-1}
koppen	Köppen–Geiger climatic zones (see Table 3) derived from *tssub1* and *precip* following Wong Hearing et al. [1].	No unit
area	Grid point area, provided for convenience for the computation of area-weighted means	m^2

languages (Python, Matlab, R etc.) and graphical user interfaces (GIS, Panoply https://www.giss.nasa.gov/tools/panoply). CSV ("comma-separated values") files contain the same data in a format that can be read using a spreadsheet programme or text editor. Files for all time slices contain the same variables and can be downloaded individually (i.e., 1 file per time slice) from https://zenodo.org/record/6620748. ZIP archives ("All_NC_files.zip" and "All_CSV_files.Zip"), also hosted on Zenodo, permit downloading all time slices at once, either as NetCDF or CSV files. File "figures.pdf" provides a graphical illustration of all variables for every time slice. Fig. 1 provides an overview of the variables included in each of the 28 files published with this article, using as an example the data for 120 Ma. Fig. 2 shows the underlying, long-term climatic trend. Fig. 3 illustrates the 28 Phanerozoic time slices (and continental configurations) included in our published dataset, using as an example the Köppen–Geiger climate classes. Table 1 describes all variables included in the dataset.

2. Experimental Design, Materials and Methods

2.1. Model description

We employed the slab version of the Fast Ocean Atmosphere Model (FOAM) version 1.5 [4], which couples an atmospheric general circulation model with a slab mixed-layer ocean model. The atmospheric component is a parallelized version of CCM2 (National Center for Atmospheric Research's Community Climate Model 2) with radiative and hydrologic physics upgraded after CCM3 version 3.2 [5]. It uses an R15 spectral resolution (4.5° × 7.5°) and 18 vertical levels. In this study, the atmosphere is coupled to a 50-meter "slab" mixed-layer ocean of resolution 1.4° × 2.8° (latitude × longitude). To parametrize the effect of ocean circulation on the oceanic heat transport, the poleward oceanic heat transport is prescribed through a diffusion coefficient tuned to provide a realistic present-day climate. Although this choice prevents from assessing the feedbacks of ocean dynamics on continental climate it allows multiple integrations that are difficult to compute with a fully-coupled model that requires integrations of several thousands of years to reach steady-state. A third model component, the coupler, ensures the robust exchange of energy and mass between the ocean and atmosphere and the simulation of sea-ice. Sea-ice is simulated using the thermodynamic component of the CSM1.4 sea-ice model, which is based on the Semtner 3-layer thermodynamic snow/ice model [6]. The coupler runs at the ocean resolution (1.4° × 2.8°). All climatic variables provided in the dataset published with this article are derived from the coupler output and thus provided at the coupler resolution. This setup of the coupled model, FOAM, has previously been used in paleoclimate studies [7,8].

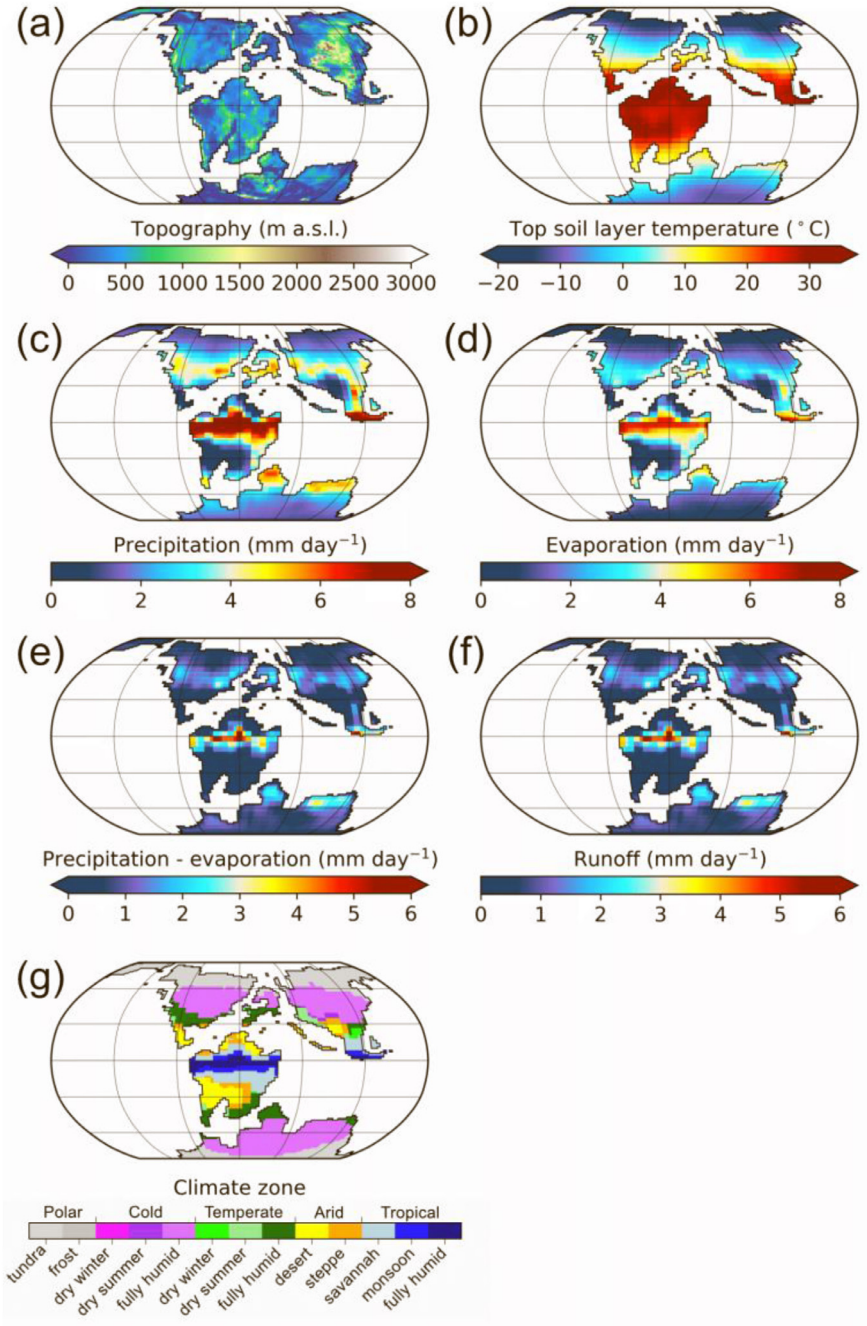

Fig. 1. Overview of the variables included in each of the 28 files published with this article, using as an example the data for 120 Ma (file "120Ma_Pohletal2022_DIB_PhaneroContinentalClimate.nc"). For variables displayed in panels (b)-(f), provided files contain seasonal (monthly) data but mean annual values (derived from the 12 monthly values) are shown here for convenience. *m a.s.l.: meters above sea level.*

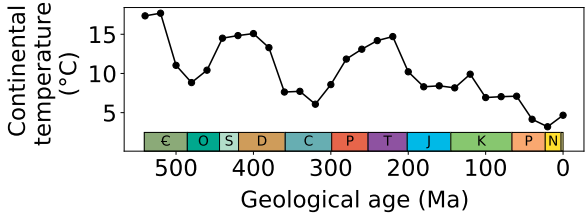

Fig. 2. Mean annual, globally-averaged continental top-layer soil temperature simulated in the FOAM model for each of the 28 Phanerozoic time slices. Є: Cambrian, O: Ordovician, S: Silurian, D: Devonian, C: Carboniferous, P: Permian, T: Triassic, J: Jurassic, K: Cretaceous, P: Paleogene, N: Neogene.

Table 2
Boundary conditions used in the FOAM model, including age of the continental reconstruction, associated solar luminosity calculated after Gough [11], atmospheric pCO_2 after Krause et al. [10], and vegetation after refs [21–23] and references therein. A null eccentricity-minimum obliquity orbital configuration is used in all simulations.

Age (Ma)	Solar luminosity (W m^{-2})	pCO_2 (ppm)	Vegetation
540	1307.89	7819	Rocky desert
520	1310.02	6584	Rocky desert
500	1312.16	4347	Rocky desert
480	1314.31	3515	Rocky desert
460	1316.46	3249	Rocky desert
440	1318.62	2774	Tundra
420	1320.79	2306	Tundra
400	1322.96	2790	Tundra
380	1325.14	1903	Tundra
360	1327.33	824	Tropical evergreen, broadleaved forest
340	1329.53	711	Tropical evergreen, broadleaved forest
320	1331.73	404	Tropical evergreen, broadleaved forest
300	1333.94	444	Tropical evergreen, broadleaved forest
280	1336.16	507	Tropical evergreen, broadleaved forest
260	1338.38	575	Tropical evergreen, broadleaved forest
240	1340.62	1823	Tropical evergreen, broadleaved forest
220	1342.86	1775	Tropical evergreen, broadleaved forest
200	1345.1	958	Tropical evergreen, broadleaved forest
180	1347.36	578	Tropical evergreen, broadleaved forest
160	1349.62	386	Tropical evergreen, broadleaved forest
140	1351.89	579	Tropical evergreen, broadleaved forest
120	1354.17	603	Tropical evergreen, broadleaved forest
100	1356.46	453	Present-day like, theoretical latitudinal bands
80	1358.75	235	Present-day like, theoretical latitudinal bands
60	1361.05	306	Present-day like, theoretical latitudinal bands
40	1363.36	279	Present-day like, theoretical latitudinal bands
20	1365.68	235	Present-day like, theoretical latitudinal bands
0	1368.0	253	Present-day like, theoretical latitudinal bands

2.2. Boundary conditions

We employed the Phanerozoic continental reconstructions of Scotese and Wright [3], which can be freely downloaded as digital elevation models, together with the associated plate model, from https://www.earthbyte.org/paleodem-resource-scotese-and-wright-2018. A description of how the paleoDEMs were constructed can be found in Scotese [9]. The atmospheric partial pressure of CO_2 was taken from the results of the recent integration of the updated version of the GEOCARB model of Krause et al. [10]. Solar luminosity was calculated for each time slice following the solar physics model of Gough [11]. We imposed different terrestrial vegetation cover types throughout the Phanerozoic to track, to first approximation, the albedo effect of the successive evolution of non-vascular plants, forests and angiosperms. Table 2 summarizes the

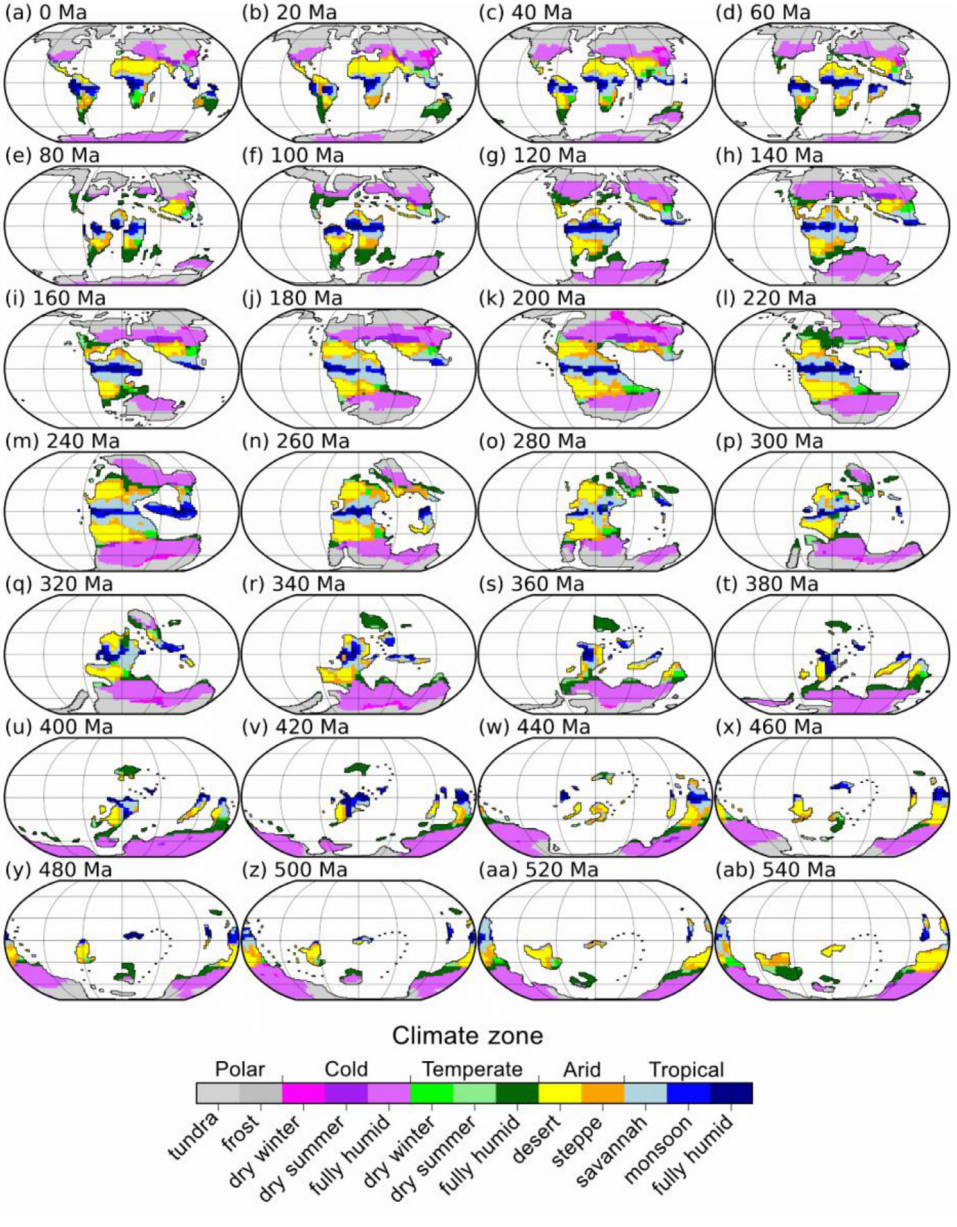

Fig. 3. Overview of the 28 Phanerozoic time slices included in our published dataset, using as an example the Köppen–Geiger climate classes (variable "koppen", see Table 1).

imposed boundary conditions. We applied a null eccentricity-minimum obliquity orbital configuration (eccentricity = 0°, obliquity = 22°), which provides equal mean annual insolation to both hemispheres with minimum seasonal contrasts. Simulations were run for 100 years until climatic equilibrium and the last 50 years were used to derive the climatic fields published here.

Table 3
Köppen–Geiger climate classes, numerical code used in files and definition, after Peel et al. [2].

Value displayed in NetCDF files	Primary climate	Secondary climate	Long name	Thresholds*
	A		Tropical	$T_{cold} \geq 18$
13		f	fully humid	$P_{dry} \geq 60$
12		m	monsoon	$P_{dry} < 60$ & $P_{dry} \geq 100–(MAP/25)$
11		w	savannah	$P_{dry} < 60$ & $P_{dry} < 100–(MAP/25)$
	B		Arid	$MAP < 10*P_{thresh}$
10		S	steppe	$MAP \geq 5*P_{thresh}$
9		W	desert	$MAP < 5*P_{thresh}$
	C		Temperate	$T_{hot} \geq 10$ & $0 < T_{cold} < 18$
8		f	no dry season	Not Cs or Cw
7		s	dry summer	$P_{sdry} < 40$ & $P_{sdry} < P_{wwet}/3$
6		w	dry winter	$P_{wdry} < P_{swet}/10$
	D		Cold	$T_{hot} \geq 10$ & $T_{cold} \leq 0$
5		f	no dry season	Not Ds or Dw
4		s	dry summer	$P_{sdry} < 40$ & $P_{sdry} < P_{wwet}/3$
3		w	dry winter	$P_{wdry} < P_{swet}/10$
	E		Polar	$T_{hot} < 10$
2		F	frost	$T_{hot} \leq 0$
1		T	tundra	$T_{hot} > 0$

* T in °C; P in mm per month; MAP in mm per year.
Summer/Winter are defined as the warmer/cooler six-month period October to March (austral summer) or April to September (boreal summer).
MAP = mean annual precipitation; MAT = mean annual temperature.
P_{dry} = precipitation of driest month; P_{wet} = precipitation of wettest month; P_{sdry} = precipitation of driest summer month; P_{swet} = precipitation of wettest summer month; P_{wdry} = precipitation of driest winter month; P_{wwet} = precipitation of wettest winter month.
T_{cold} = temperature of the coldest month; T_{hot} = temperature of hottest month. If 70 % MAP in winter, $P_{thresh} = 2 \times MAT$; if 70% MAP in summer, $P_{thresh} = (2 \times MAT) + 28$; else, $P_{thresh} = (2 \times MAT) + 14$. P_{thresh} is therefore temperature-dependent.

2.3. Köppen–Geiger classification

Köppen–Geiger climate classes (Fig. 3) were derived from the simulated monthly temperature and precipitation fields (Fig. 1) following Peel et al.'s [2] revised classification (Table 3) using Wong Hearing et al.'s [1] R script. The Köppen–Geiger climate classification scheme has three levels [12–14]. The first level describes the primary climate class (tropical, arid, temperate, cold, and polar) defined by temperature thresholds. The second level is a precipitation modifier of the main climate class, with the exception of arid climates which are subdivided by a second temperature threshold. The third layer describes temperature variation within the main class, and is only applied to three of the five climate classes (arid, temperate, and cold climates). Because of the loose constraints on boundary conditions employed here (e.g. median orbital configuration), we consider it appropriate only to use the first two layers of the Köppen–Geiger climate classification scheme with these data, though the R script allows implementation of one, two, or all three levels [1].

3. Limitations

Our paleoclimate reconstructions bear two main sources of uncertainty, namely the model structural biases and the hypotheses we made regarding the boundary conditions of our simulations.

3.1. Model limitations

When compared with present-day climatologies, FOAM-slab depicts near-surface air temperatures that are overestimated over Antarctica, relating to the absence of explicit Antarctic circum-polar current. The model also underestimates continental temperatures in the Northern Hemisphere at high latitudes, which could be related to too strong snow-albedo feedbacks. How these biases translate into past climate remains to be determined, as much of Phanerozoic periods considered here are ice-free. Similar to many modern climate models, FOAM-slab also underestimates rainfall patterns in the neotropics, and conversely overestimate them over equatorial Africa. These patterns are linked to poor water recycling through vegetation feedbacks as well as a misplaced intertropical convergence zone (ITCZ), a pattern that also exists with recent fully-coupled Earth System Models [15]. Biases also occur over topographic areas, as the spatial resolution of the atmospheric component does not permit representation of fine variations in terrain.

3.2. Uncertainties in the model boundary conditions

Reconstruction of past atmospheric CO_2 concentrations is uncertain. Here we used values obtained from the GEOCARBSULFOR model [10]. For the Cenozoic, these values are likely underestimated, as most recent reconstructions depict pCO_2 far higher than 400 ppmv from the Paleogene to the late Miocene [16]. Therefore, our reconstructions for the last 80 Myrs are likely too cold.

Another source of uncertainty lies in the choice of the orbital parameters (eccentricity, obliquity and precession), which together define the trajectory of the Earth around the Sun and modulate the distribution of incoming solar energy in space (along the latitudes) and time (during the year). Since there are no numerical solutions for insolation quantities beyond 250 Ma [17,18], and because the 20-Myr time steps are large compared to the timescales of orbital variability, choice was made to use the same orbital parameters for all simulations. The null-eccentricity low-obliquity configuration induces less marked seasonal cycles as well as overall less energy received yearly by polar regions, and our simulations cannot represent the climatic variability linked to combined effects of eccentricity, obliquity and precession on the top-of-atmosphere radiative budget.

Finally, uncertainties in the position of the landmasses, in the geometry of the coastlines and also in the estimation of past topography/bathymetry, increase with geological age [1,3,19,20]. The impact of this uncertainty on our ensemble of Phanerozoic simulations remains difficult to quantify.

Ethics Statements

No statement applies.

CRediT Author Statement

Alexandre Pohl: Conceptualization, Data curation, Formal analysis, Funding acquisition, Investigation**,** Methodology, Project administration, Resources, Software, Validation, Visualization, Writing - original draft, Writing - review & editing **Thomas Wong Hearing:** Conceptualization, Data curation, Formal analysis, Funding acquisition, Investigation, Methodology, Project administration, Resources, Software, Validation, Visualization, Writing - original draft, Writing - review & editing **Alain Franc:** Formal analysis, Investigation, Methodology, Resources, Software, Writing -

review & editing **Pierre Sepulchre:** Formal analysis, Investigation, Methodology, Resources, Software, Validation, Writing - review & editing **Christopher R. Scotese:** Investigation, Methodology, Resources, Writing - review & editing

Declaration of Competing Interest

The authors declare that they have no known competing financial interests or personal relationships that could have appeared to influence the work reported in this paper.

Acknowledgments

This project has received funding from the European Union's Horizon 2020 research and innovation programme under the Marie Sklodowska-Curie grant agreement No. 838373 (to AP) and from Ghent University Special Research Fund (BOF) Fellowship 01P12419 (to TWWH). Calculations were performed using HPC resources from DNUM CCUB (Centre de Calcul de l'Université de Bourgogne). We thank I. N. Bindeman (U. Oregon, OR, USA), for comments that improved this manuscript.

References

[1] T.W. Wong Hearing, A. Pohl, M. Williams, Y. Donnadieu, T.H.P. Harvey, C.R. Scotese, P. Sepulchre, A. Franc, T.R.A. Vandenbroucke, Quantitative comparison of geological data and model simulations constrains early Cambrian geography and climate, Nat. Commun. 12 (2021) 3868, doi:10.1038/s41467-021-24141-5.
[2] M.C. Peel, B.L. Finlayson, T.A. McMahon, Updated world map of the Köppen-Geiger climate classification, Hydrol. Earth Syst. Sci. 11 (2007) 1633–1644, doi:10.5194/hess-11-1633-2007.
[3] C.R. Scotese, N. Wright, PALEOMAP Paleodigital Elevation Models (PaleoDEMS) for the Phanerozoic (PALEOMAP Project, 2018), (2018). https://www.earthbyte.org/paleodem-resource- scotese-and-wright-2018/.
[4] R.L. Jacob, in: Low frequency variability in a simulated atmosphere-ocean system, University of Wisconsin Madison, 1997, p. 170. https://ftp.mcs.anl.gov/pub/People/jacob/RLJdissertation.ps.gz. PhD thesispages.
[5] J.T. Kiehl, J.J. Hack, G.B. Bonan, B.A. Boville, D.L. Williamson, P.J. Rasch, The national center for atmospheric research community climate model: CCM3, J. Clim. 11 (1998) 1131–1149, doi:10.1175/1520-0442(1998)011⟨1131:TNCFAR⟩2.0.CO;2.
[6] A.J. Semtner, A Model for the Thermodynamic Growth of Sea Ice in Numerical Investigations of Climate, J. Phys. Oceanogr. 6 (1976) 379–389, doi:10.1175/1520-0485(1976)006⟨0379:amfttg⟩2.0.co;2.
[7] E. Nardin, Y. Goddéris, Y. Donnadieu, G.Le Hir, R.C. Blakey, E. Pucéat, M. Aretz, Modeling the early Paleozoic long-term climatic trend, Bull. Geol. Soc. Am. 123 (2011) 1181–1192, doi:10.1130/B30364.1.
[8] Y. Goddéris, Y. Donnadieu, G.Le Hir, V. Lefebvre, E. Nardin, The role of palaeogeography in the Phanerozoic history of atmospheric CO2 and climate, Earth-Science Rev 128 (2014) 122–138, doi:10.1016/j.earscirev.2013.11.004.
[9] C.R. Scotese, An Atlas of Phanerozoic Paleogeographic Maps: The Seas Come In and the Seas Go Out, Annu. Rev. Earth Planet. Sci. 49 (2021) 679–728, doi:10.1146/annurev-earth-081320-064052.
[10] A.J. Krause, B.J.W. Mills, S. Zhang, N.J. Planavsky, T.M. Lenton, S.W. Poulton, Stepwise oxygenation of the Paleozoic atmosphere, Nat. Commun. 9 (2018) 4081, doi:10.1038/s41467-018-06383-y.
[11] D.O. Gough, Solar interior structure and luminosity variations*, Sol. Phys. 74 (1981) 21–34, doi:10.1007/BF00151270.
[12] W. Köppen, E. Volken, S. Brönnimann, The thermal zones of the Earth according to the duration of hot, moderate and cold periods and to the impact of heat on the organic world, Meteorol. Zeitschrift. 20 (2011) 351–360, doi:10.1127/0941-2948/2011/105.
[13] W. Köppen, Die Wärmezonen der Erde, nach der Dauer der heissen, gemässigten und kalten Zeit und nach der Wirkung der Wärme auf die organische Welt betrachtet, Meteorol. Zeitschrift. (1884), doi:10.1127/0941-2948/2011/105.
[14] F. Rubel, M. Kottek, Comments on: "The thermal zones of the Earth" by Wladimir Köppen (1884), Meteorol. Zeitschrift. 20 (2011) 361–365, doi:10.1127/0941-2948/2011/0285.
[15] P. Sepulchre, A. Caubel, J.-B. Ladant, L. Bopp, O. Boucher, P. Braconnot, P. Brockmann, A. Cozic, Y. Donnadieu, V. Estella-Perez, C. Ethé, F. Fluteau, M.-A. Foujols, G. Gastineau, J. Ghattas, D. Hauglustaine, F. Hourdin, M. Kageyama, M. Khodri, O. Marti, Y. Meurdesoif, J. Mignot, A.-C. Sarr, J. Servonnat, D. Swingedouw, S. Szopa, D. Tardif, IPSL-CM5A2. An Earth System Model designed for multi-millennial climate simulations, Geosci. Model Dev. 13 (2020) 3011–3053, doi:10.5194/gmd-13-3011-2020.

[16] J.W.B. Rae, Y.G. Zhang, X. Liu, G.L. Foster, H.M. Stoll, R.D.M. Whiteford, Atmospheric CO2 over the past 66 million years from marine archives, Annu. Rev. Earth Planet. Sci. 49 (2021) 609–641, doi:10.1146/annurev-earth-082420-063026.
[17] J. Laskar, P. Robutel, F. Joutel, M. Gastineau, A.C.M. Correia, B. Levrard, A long-term numerical solution for the insolation quantities of the Earth, Astron. Astrophys. 428 (2004) 261–285 http://gateway.webofknowledge.com/gateway/Gateway.cgi?GWVersion=2&SrcAuth=mekentosj&SrcApp=Papers&DestLinkType=FullRecord&DestApp=WOS&KeyUT=000225334900034.
[18] J. Laskar, A. Fienga, M. Gastineau, H. Manche, La2010: A new orbital solution for the long-term motion of the Earth, Astron. Astrophys. 532 (2011), doi:10.1051/0004-6361/201116836.
[19] A. Kocsis, C.R. Scotese, Mapping paleocoastlines and continental flooding during the Phanerozoic, Earth-Science Rev (2020), doi:10.1016/j.earscirev.2020.103463.
[20] R.D. Müller, M. Sdrolias, C. Gaina, B. Steinberger, C. Heine, Long-term sea-level fluctuations driven by ocean basin dynamics, Science 319 (2008) 1357–1362 http://www.sciencemag.org/cgi/doi/10.1126/science.1151540.
[21] G.Le Hir, Y. Donnadieu, Y. Goddéris, B. Meyer-Berthaud, G. Ramstein, R.C. Blakey, The climate change caused by the land plant invasion in the Devonian, Earth Planet. Sci. Lett. 310 (2011) 203–212, doi:10.1016/j.epsl.2011.08.042.
[22] P. Porada, T.M. Lenton, A. Pohl, B. Weber, L. Mander, Y. Donnadieu, C. Beer, U. Pöschl, A. Kleidon, High potential for weathering and climate effects of non-vascular vegetation in the Late Ordovician, Nat. Commun. 7 (2016) 12113, doi:10.1038/ncomms12113.
[23] C.V. Rubinstein, P. Gerrienne, G.S. de la Puente, R.A. Astini, P. Steemans, Early Middle Ordovician evidence for land plants in Argentina (eastern Gondwana), New Phytol 188 (2010) 365–369, doi:10.1111/j.1469-8137.2010.03433.x.